Ferromagnetic exchange field stabilized antiferromagnetic ordering in a cuprate superconductor

Biswajit Dutta and A. Banerjee
UGC-DAE Consortium for Scientific Research, University Campus, Khandwa Road, Indore-452001, India

(Received 5 November 2021; revised 10 October 2022; accepted 11 October 2022; published 31 October 2022)

We report experimental evidence of the formation of antiferromagnetic clusters well within cuprate superconductor $La_{1.85}Sr_{0.15}CuO_4$ (LCu) in a composite made of LCu and ferromagnet $La_{0.6}Sr_{0.4}CoO_3$ (LCo). It is found that the exchange field of LCo suppresses the dynamic antiferromagnetic spin fluctuation of LCu and short-range-ordered superparamagnetic type antiferromagnetic (AFM) clusters are formed at the cost of superconducting volume fraction. With the help of linear and nonlinear ac-susceptibility measurements, we show evidence of thermal blocking of these antiferromagnetic clusters. Further, we show that the shrank superconducting volume fractions undergo the quantum size effect (QSE) and follow DeGennes-Tinkham theory on the finite size effect of a superconductor. These give a clear indication that the antiferromagnetic spin fluctuation can be a mediator of electron pairing in cuprate superconductors.

DOI: 10.1103/PhysRevB.106.134520

I. INTRODUCTION

One of the long-lived mystery associated with high-temperature cuprate superconductors is the origin of coherent electron pairing in these compounds. The magnetic state of a parent cuprate is a 3D Neel antiferromagnet (AFM). After doping holes or electrons, the ordered antiferromagnetic state is destroyed and a superconducting state emerges [1]. However, the existence of the AFM type spin correlation is revealed throughout the hole or electron doped phase diagram (including the doping region where superconductivity exists) and depending on the dynamical nature of the AFM correlation, the strength of superconductivity is decided [1–7]. It is also observed that when the superconducting state is destroyed by doping or by applying a very high magnetic field, then the emergence of the AFM-like state is obser ved, for example, neodymium (Nd) doping in $La_{1.85}Sr_{0.15}CuO_4$ (LCu) destroys the superconducting state and results in antiferromagnetic type CDW phase [8–10]. Further, the suppression of superconductivity and the emergence of the charge density wave (CDW) phase or AFM state are also revealed in ferromagnet (FM) and cuprate superconductor heterostructures at the normal conditions (or without imposing any extreme condition or doping in the superconductor) [11–18]. This characteristic behavior indicates a close correlation between the AFM ordering and coherent electron pairing mechanism in cuprate superconductors, which has also opened up a new perspective to understand the superconducting pairing mechanism of cuprate superconductors. Therefore a detailed study of cuprate superconductor in proximity to FM systems are required to get further knowledge about the involvement of antiferromagnetic type spin correlation in the pairing mechanism. Mostly, such studies on oxide superconductor and ferromagnet (SC/FM) are based on $YBa_2Cu_3O_7$ (YBCO) and $La_{0.7}Sr0.3MnO_3$ (or $La_{0.7}Ca0.3MnO_3$). However, the problem associated with these YBCO based SC/FM heterostructures is high probability of disruption of CuO chain (which act as charge reservoir in YBCO) across the interface. As a result of that, the hole concentration of YBCO gets modified, changing the physical property in the bulk-like manner unrelated to interface physics [19–22]. It has been observed that the SC/FM interfaces consisting of $La_{1.85}Sr_{0.15}CuO_4$ (LCu) as a superconductor does not show any dominant charge transfer or orbital reconstruction phenomena to take place across the interface [23–26] and maintained their charge state intact with respect to the parent ingredient. Hence, LCu based (or LCu type, i.e., $Pr_{1-x}Ce_xCuO_4$ [23]) FM/SC composites (or bilayer) are ideal to study the effects of the exchange field [23], as well as the interfacial strain effect on the magnetic properties of cuprate superconductors [23–26].

Here, we present a study on composites made of superconductor LCu and a ferromagnet $La_{0.6}Sr_{0.4}CoO_3$ (LCo) to explore the effect of exchange bias field on the hole doped cuprate superconductor. LCo is chosen as a ferromagnetic counterpart because it shows long-range ferromagnetic ordering and large magnetocrystalline anisotropy [27–30], which can facilitate a substantial amount of exchange bias field on the spins of a copper atom of LCu. In this respect, it has an advantage over manganites ($La_{0.7}Sr_{0.3}MnO_3$, $La_{0.7}Ca_{0.3}MnO_3$ [24–26]) to explore the effect of the exchange field on cuprate superconductors. We show that the dynamic antiferromagnetic spin fluctuation of LCu [8–10,31–33] is suppressed due to the magnetic exchange field of LCo and the short-range-ordered AFM phase is developed at the cost of superconducting volume fraction. As a result, the bulk superconducting region shrank to finite size clusters, and the quantum size effect (QSE) of the superconductor appears, without any reduction in the crystallite size of the superconductor. The exchange field amplitude on LCu is tuned by changing the effective interface as well as by the dc magnetic field. The effective interface is varied by following several processes like reducing (or increasing) the particle

size, decreasing (or enhancing) the concentration of LCo in the LCu matrix [34], and grinding the composite pallet.

We have used Linear and nonlinear ac-susceptibility measurements to study the proximity effect induced change of the magnetic state of a superconductor in a SC/FM interface. Nonlinear susceptibilities are found to be a very effective tool in determining various characteristics of a type-2 superconductor, such as to identify the onset point of an irreversible flux motion, the nature of flux dynamic, and also very effective in determining various critical thermodynamical parameters (like critical current, critical field, and critical temperature) [35–38]. This technique is also very effective in unambiguously distinguishing various metastable states like spin glass, cluster glass, and superparamagnet [39–42] and also in the establishing the nature of the magnetic ground state (like ferromagnetic or antiferromagnetic) [43,44].

In a composite (or in a heterostructure), the interplay between different electronic ground states are modulated through the extended interface effect, but in the case of oxide heterostructures, oxygen stoichiometry plays a big role in modifying the physical property which is unrelated to interface physics. Hence it is very important to determine the oxygen stoichiometry (which defines the spin state) of the ingredients with respect to their parent compounds for a conclusive discrimination between the phenomena related to interface effect and the phenomena associated with the degradation of oxygen stoichiometry. We have proposed a method to determine the spin state of a ferromagnet and a hole concentration of a superconductor in a SC/FM composite system by using the low field magnetic ac-susceptibility technique and XRD measurement, which is already published in Ref. [34] and briefly discussed here.

II. SAMPLE PREPARATION AND CHARACTERIZATION

The parent ingredient LCu and LCo is prepared by a pyrophoric method. Then the composites are prepared by solid state reaction method, preparation technique is more elaborately explained in Ref. [34]. The precursor of LCo just obtained after pyrophoric chemical reaction is annealed at different temperatures, viz. 950 °C, 900 °C, and 850 °C to obtained three different crystalline size (CS) which are nomenclatured as LCo950, LCo900, and LCo850 respectively $[(CS)_{LCo850} < (CS)_{LCo900} < (CS)_{LCo950}]$. Then 76 weight percentage of LCu and 24 weight percentage of LCo950 is mixed, palletized at comparatively high pressure [i.e., 150 kilo-Newton (kN)] and heated at 800 °C to prepare composite A1. In the similar way, A2 and A3 are prepared by mixing LCo900 and LCo850 with LCu, respectively. The concentration of LCo850 is also varied in LCu matrix to change the effective interface between LCu and LCo. In this case, LCu and LCo850 is mixed at different weight ratio like 76:24, 85:15, and 95:5 and these composites are nomenclatured as A3, A4, and A5, respectively. The parent ingredients are independently grinned palletized at similar pressure (i.e., 150 kN) and annealed at same temperature (i.e., 800 °C) for comparison purposes. The weight percentage detail of the corresponding parent ingredient present in the composites (i.e., A1, A2, A3, A4, A5) and detailed nomenclature of all composites along with the crystalline size of parent LCu and

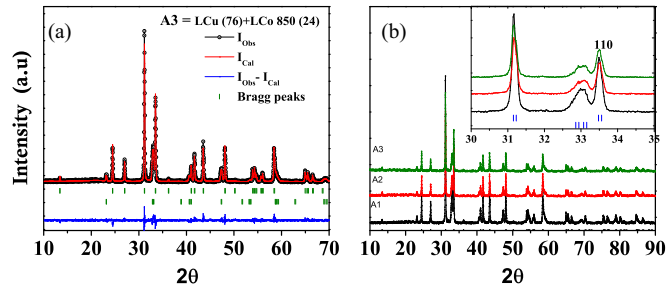

FIG. 1. (a) Rietveld refinement of composite A3. (b) XRD plot of all composites A1, A2, and A3 (Inset shows the region 30°–35° shows the maximum intensity peak region).

LCo are provided in Table I. The crystalline sizes of the ferromagnet and the superconductor are calculated from the XRD patterns as well as from transmission electron microscopy (TEM) measurements.

A. Structural characterization: XRD

X-ray diffraction (XRD) measurements are performed in Bruker x-ray diffractometer from 10°–90° at an interval of 0.02°. Figure 1(a) shows the two-phase Rietveld refinement of the composite A3 and Fig. 1(b) shows the XRD pattern of A1, A2, and A3, respectively. Figure 2(a) shows the Rietveld refinement of the composite A5 and the combined plot of the XRD spectrum of A3, A4, and A5 composite are shown in Fig. 2(b) for comparison. The phase fractions and other structural details obtained from two phase Rietveld refinement are given in Table II.

The lattice parameters of LCu obtained after the two phase Rietveld refinement of all composites (i.e., A1 to A5) do not show any significant change, which indicates the c/a ratio or the orthorhombic distortion of LCu remain the same for all composites. This indicates that there is no change in the hole concentration of LCu [8]. The crystalline size of LCu and LCo is calculated using Williamson-Hall (W-H) analysis. The hole concentration of parent LCo is determined by Iodometric titration method. The chemical formula obtained from these results are as follows; like for LCo950, LCo900, and LCo850 it is $La_{0.6}Sr_{0.4}CoO_{2.97}$, $La_{0.6}Sr_{0.4}CoO_{2.99}$, and $La_{0.6}Sr_{0.4}CoO_{3.01}$, respectively. From this chemical formula, the concentration ratio of Co^{+3} and Co^{+4} ions can be calculated very easily and this ratio is further used to calculate the theoretical values of the effective magnetic moment (μ_{eff}) and

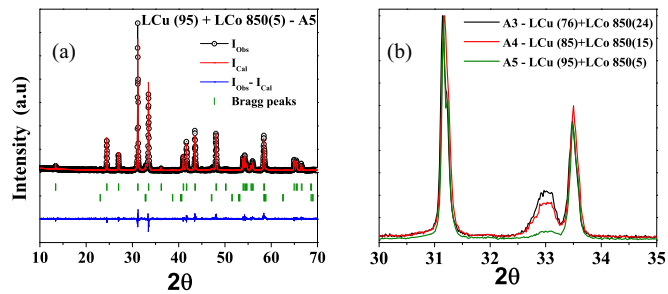

FIG. 2. (a) Rietveld refinement of composite A5. (b) XRD plot of all composites A3, A4, and A5.

TABLE I. List of composites and crystalline size details.

Composite Name	LCu [weight%] + LCo (annealing Temperature) [Weight%]	Average crystalline Size of LCo (nm)
A1	LCu[76%]+LCo(950)[24%]	69 (nm)
A2	LCu[76%]+LCo(900)[24%]	47 (nm)
A3	LCu[76%]+LCo(850)[24%]	27 (nm)
A4	LCu[85%]+LCo(850)[15%]	27 (nm)
A5	LCu[95%]+LCo(850)[5%]	27 (nm)

saturation moment of the corresponding LCo. Experimentally the value of μ_{eff} has been calculated from the Curie-Weiss fitting in the paramagnetic region of LCo and the obtained value is compared with the theoretical effective magnetic moment value of LCo [$(\mu_{\text{eff}})_{\text{expt}} = 4.33 \pm 0.01$]. As LCu is a Pauli paramagnet, the moment value above superconducting onset temperature is found around 10^{-6} emu (much smaller than the Curie-Weiss moment value of LCo), and it is constant for up to room temperatures. Therefore the effective magnetic moment value of parent LCo and the corresponding composites has to be same provided there is no change of hole concentration or chemical reaction. We have used this concept to determine the spin state (i.e., hole concentration) of LCo present in the composite [34].

B. Transmission electron microscopy (TEM)

A transmission electron microscopy (TEM) image of composite A3 is shown in Fig. 3(a). The high resolution transmission electron microscopy (HRTEM) image is shown in Figs. 3(b)–3(d). The high resolution images are depicting that the crystallites of LCo are connected and combined with the crystallite of LCu, respectively. The fringes of the marked lattice spacing of 0.5 nm, correspond to LCo. Figure 3(d) indicates a very sharp interface, which clearly depicts that there is no intermixing between LCu and LCo. We have performed similar TEM and HRTEM measurements at various places of A3 and also performed high angle annular dark field imaging (i.e., elemental scan), see Sec. A in Ref. [45] for more elaborate explanation.

TABLE II. Best fitted parameters, SG-space group, PF-phase fraction, a, b, and c are lattice parameters.

Material	SG	a (Å)	b (Å)	c (Å)	PF	R_f
(LCu)	$I4/mmm$	3.78(9)	3.78(9)	13.20(5)	NA	1.35
(LCo850)	$R\text{-}3c$	5.44(5)	5.44(5)	13.22(5)	NA	1.44
(LCo900)	$R\text{-}3c$	5.44(6)	5.44(6)	13.21(7)	NA	1.44
(LCo950)	$R\text{-}3c$	5.44(3)	5.44(3)	13.20(5)	NA	1.44
A1(LCu)	$I4/mmm$	3.78(9)	3.78(9)	13.20(3)	76	1.47
A1(LCo)	$R\text{-}3c$	5.44(2)	5.44(2)	13.20(9)	24	1.47
A2/(LCu)	$I4/mmm$	3.78(3)	3.78(3)	13.20(9)	76	1.44
A2/(LCo)	$R\text{-}3c$	5.44(6)	5.44(6)	13.21(5)	24	1.44
A3/(LCu)	$I4/mmm$	3.78(2)	3.78(2)	13.20(3)	76	1.8
A3/(LCo)	$R\text{-}3c$	5.44(1)	5.44(1)	13.21(7)	24	1.8
A4/(LCu)	$I4/mmm$	3.78(4)	3.78(4)	13.20(8)	86	1.6
A4(LCo)	$R\text{-}3c$	5.44(9)	5.44(9)	13.21(9)	14	1.6
A5/(LCu)	$I4/mmm$	3.78(6)	3.78(6)	13.20(9)	95.9	1.87
A5/(LCo)	$R\text{-}3c$	5.44(8)	5.44(8)	13.22(1)	4.1	1.87

III. EXPERIMENTAL DETAILS

The low field linear and nonlinear magnetic ac-susceptibility measurements have been performed using a homemade ac susceptometer, which can be operated down to 4 from 300 K and the measurements can be done in both cooling and heating cycle with a temperature accuracy better than 1 mK. The estimated sensitivity of the setup is $\sim 10^{-7}$ emu [46]. The higher dc field (>200 Oe) superimposed ac-susceptibility measurements are performed in MPMS-XL (M/S, Quantum Design).

A. Ac-susceptibility measurement

The magnetic property of the composite has been studied by extensive use of ac-susceptibility measurement which is capable to probes the spin dynamic at very low field. The magnetization (m) can be expanded with respect to the applied ac field $h_{\text{ac}}(h)$ as

$$m = m_0 + \chi_1 h + \chi_2 h^2 + \chi_3 h^3 + \chi_4 h^4 + \cdots \quad (1)$$

$\chi_1 (\approx \delta m/\delta h)$ is linear susceptibility and χ_2, χ_3, χ_4, ...are nonlinear susceptibilities. These nonlinear susceptibilities contain many fruitful information but magnitude of these are much smaller (couple of order) than the linear susceptibility, therefore they are difficult to measure from normal dc magnetization measurement, but these nonlinear susceptibilities can be easily measured using high sensitive ac-susceptibility measurements [47]. If the magnetization has an inversion symmetry with respect to the applied ac field (h_{ac}) then all the even order susceptibilities, like $\chi_2 (\approx \delta^2 m/\delta^2 h)$, $\chi_4 (\approx \delta^4 m/\delta^4 h)$ are zero without any externally applied dc field (i.e., at $h_{\text{dc}} = 0$ Oe) like paramagnetic and antiferromagnetic materials, but when the inversion symmetry breaks with

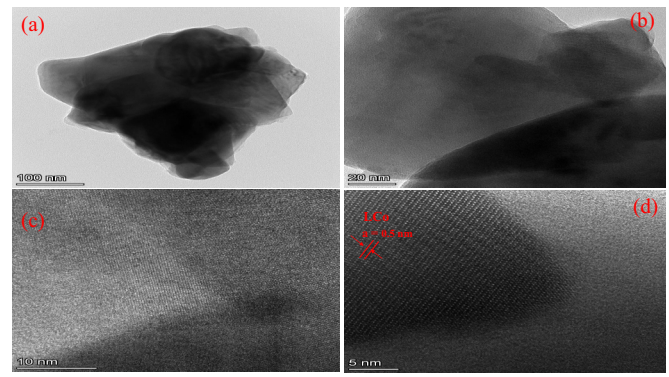

FIG. 3. HRTEM image of composite A3 is shown at various resolutions.

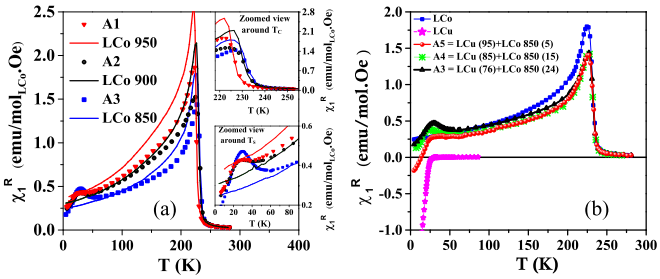

FIG. 4. (a) The combined temperature-dependent plot of $\chi_1^R(T)$ for the composite A1 (red triangle) and LCo950 (red line), composite A2 (black circle), and LCo900 (black line), composite A3 (blue rectangular box), and LCo850 (blue line). (Top inset) Zoomed view around ferromagnetic to paramagnetic transition temperature T_C. (Bottom inset) Zoomed view around superconducting onset temperature [$T_{S(\text{onset})}$]. (b) The combined temperature-dependent plot of A3, A4, A5, LCu, and LCo depicted. All the measurements are done in an ac field of amplitude 3 Oe and frequency 231.1 Hz.

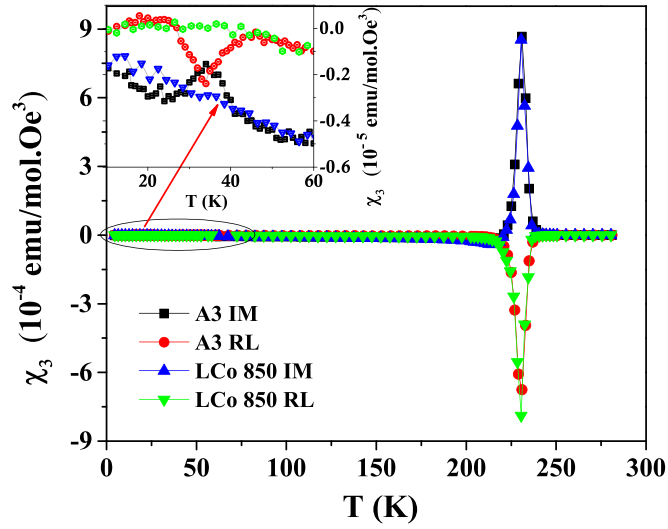

FIG. 5. The temperature-dependent mole normalized real (RL) and imaginary (IM) parts of χ_3 of composites A3 and LCo850. (Inset) Zoomed view of the anomalous region around superconducting onset [$T_{S(\text{onset})}$]. The measurements are performed at ac field $h_{\text{ac}} = 3$ Oe and frequency $f = 231.1$ Hz.

respect to the sign of h_{ac} then χ_2, χ_4, etc., all the even order susceptibility shows a finite value (at $h_{\text{dc}} = 0$ Oe), like in the case of ferromagnets or a ferrimagnetic state [43,47,48].

Third-order susceptibility (χ_3) is a very useful tool to discriminate between various metastable states [like spin glass (SG), superparamagnet (SPM), etc.] ably [40,41,49–51]. For example, if there are interparticle interactions, then the frequency-dependent nature of χ_1^R(T) for an SPM system will give similar result as that of an SG system. Hence, in this type of situation, it becomes difficult to discriminate between SG and SPM by looking only at the frequency-dependent χ_1^R(T) result [50]. Whereas across spin glass transition a negative cusp in χ_3 is observed which is correlated with the divergence of the Edward-Anderson order parameter, but in the case of SPM, this type of divergence is absent [40,41,49]. χ_3 is also found as a very effective tool in determining the universality class of the ferromagnet i.e., to study the nature of magnetic ground state of the corresponding ferromagnet [43,52]. Therefore the behavior of χ_3 around ferromagnetic to paramagnetic transition (T_C) is very important in deciding the nature of magnetic interaction or the nature of the magnetic ground state of a ferromagnet.

IV. RESULTS AND DISCUSSIONS

The combined temperature-dependent plot of mole normalized χ_1^R(T) (the real part of first-order susceptibility) of A1, A2, and A3 as well as their respective ferromagnetic constituent is shown in Fig. 4(a). χ_1^R(T) of the composite A1 is indicated by a down red triangle and χ_1^R(T) plot of the corresponding ferromagnet LCo950 is indicated by the red line. Similarly, black and blue colors (symbols and line) describes the same for composites A2 and A3, respectively. All measurements are performed in the heating cycle. The normalization of $\chi_1^R(T)$ is performed with respect to the mole fraction of LCo as obtained from the Rietveld refinement of the XRD patterns [34]. The zoomed view of $\chi_1^R(T)$ around FM T_C is shown in the upper inset of Fig. 4(a), it is observed that around T_C and above it the χ_1^R(T) value of the composite matches with the χ_1^R(T) value of the corresponding ferromagnet present in that. These observation indicates that the Curie temperature (θ_C) and effective magnetic moment (μ_{eff}) of the composites and the corresponding parent LCo are the same (θ_C and μ_{eff} have been calculated from the Curie-Weiss fitting of the paramagnetic region of $\chi_1^R(T)$ graph [34]). It suggests the magnetic structure (or oxygen stoichiometry) of LCo in the composites remain the same with respect to their parent LCo. The similar conclusion has been drawn from χ_3 as shown later (Fig. 5). Hence the anomaly around the superconducting onset temperature $T_{S(\text{onset})}$, shown in the bottom inset of Fig. 4(a) indicates the modification of the magnetic state of LCu due to close proximity of LCo. The anomaly is more prominent in the case of A3 than A2 and A1, because A3 consists of smaller ferromagnetic particle LCo850, hence it has a larger surface-to-volume ratio than LCo900 and LCo950, due to this reason the effective interface between LCu and LCo is larger in the case of A3 than A1 and A2. Therefore the above observation depicts the anomaly around $T_{S(\text{onset})}$ is an interface effect.

To cross-check the statement related to the interface effect, the ratio of LCu and LCo is changed in composites A4 and A5 (as mentioned before) to vary the number of LCo grains sprinkled across LCu domain, which also changes the effective interface between LCu and LCo. Figure 4(b) shows the comparative normalized χ_1^R(T) plot of composites A3, A4, and A5, along with them the normalized χ_1^R(T) graph of parent LCo and LCu is also shown for comparison purpose. The onset temperature of superconductivity [$T_{S(\text{onset})}$] of LCu is observed around 32 K and above $T_{S(\text{onset})}$, $\chi_1^R(T)$ shows Pauli paramagnetic behavior. The paramagnetic to ferromagnetic transition temperature (T_C) of LCo850 is observed around 233 K. The anomalous hump in χ_1^R(T) around the superconducting transition gets suppressed with the reduction of the LCo850 concentration in the LCu matrix [shown in Fig. 4(b)], like for A4, the amplitude of the peak value suppresses and

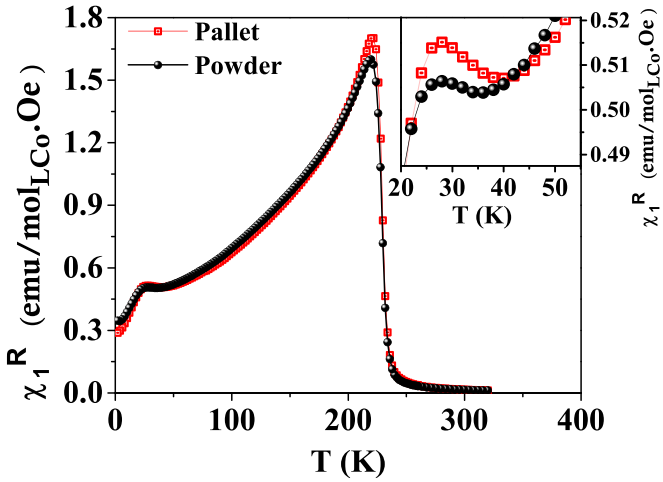

FIG. 6. The plot of $\chi_1^R(T)$ against temperature for A2 composite in two different conditions. The red square block shows the result for pallet and the black circle for the powder samples. Inset shows the zoomed view of the anomalous region. The measurements are performed at ac $h_{ac} = 3$ Oe and frequency $f = 231.1$ Hz.

becomes almost flat for A5. From the Curie-Weiss fitting in the paramagnetic region, the values of μ_{eff} and θ are obtained around 4.28 μ_b and 233 K, respectively. The Hopkinson peak amplitude [i.e., the peak in χ_1^R(T) graph just below FM T_C] for all the composites remains the same, which indicates the magnetic domain size of LCo is same in all composites. Thus the observed anomaly suppresses in similar manner as that of Fig. 4(a), which is an indication that the anomaly in χ_1^R(T) measurement is an interface driven phenomenon.

The mole normalized χ_3 plot of composite A3 and the corresponding ferromagnet is shown in Fig. 5 (the number of moles of LCo present in the composite is used to normalize the χ_3 graph of the composite). It shows that the nature of χ_3 (both real and imaginary parts) remain the same for the composite and the ferromagnet except around the superconducting onset temperature [$T_{S(\text{onset})}$], which gives the direct indication that the magnetic state of the ferromagnet present in the composite remain the same as that of the parent ferromagnet.

The interface effect is further verified by measuring the $\chi_1^R(T)$ behavior of a composite pallet (A2) and the powder specimen of same composite; the comparative plot is shown in Fig. 6. The intergranular connection reduces after making powder of the composite pallet and hence the effective interface between LCu and LCo reduces. The difference between the $\chi_1^R(T)$ plot of powder and pallet around $T_{S(\text{onset})}$ can be clearly distinguished from the inset. For powder, the hump is suppressed as a result of the reduction of an effective interface but there is no change in the critical temperature of the ferromagnet. So all these measurements unambiguously show that when the effective interface reduces then the anomaly around $T_{S(\text{onset})}$ also decreases, which clearly proves the phenomena is an interface effect.

The gradual decrease of the diamagnetic fraction below $T_{S(\text{onset})}$ while increasing the effective interface is evident in Fig. 4(b). The crystallite size and the lattice parameter of LCu (and LCo) remain almost same for all composites (evident from the XRD graph). The magnetic ac-susceptibility measurement depicts the demagnetization factor and spin state of LCo also remain the same for all the composites (evident from the equal values of the Hopkinson peak height at 226 K and paramagnetic moment), so the decrement of diamagnetic phase fraction is not related to the degradation of hole concentration or structural distortion of either LCu or LCo. This indicates a possibility that there has developed some kind of magnetic interaction between LCu and LCo across the interface, which causes the observed changes in the magnetic state of LCu [like the decrease in diamagnetic susceptibility and excess susceptibility across $T_{S(\text{onset})}$]. Otherwise, if it is due to the change of magnetic state of LCo then the change could have been observed around T_C with increasing or decreasing concentration of LCo [in Fig. 4(b)]. Along with that, above $T_{S(\text{onset})}$, the magnetization strength of LCu (i.e., Pauli paramagnetic) is much smaller than LCo (ferromagnetic), which can not affect the magnetic state of LCo but the vice versa is highly probable. Hence, it can be concluded that the magnetic state of LCu is getting affected because of its proximity to LCo, without any change in the chemical composition of the constituents in the composites.

To reveal the nature of the perturbed magnetic state of LCu and also the type of magnetic interaction across the interface, the higher order (i.e., second order-χ_2 and third order-χ_3) ac-susceptibility measurements are performed because of their unique ability to distinguish between various magnetic state (as previously discussed). Around $T_{S(\text{onset})}$, χ_3^R shows a dip like feature (shown in the inset of Fig. 5) and around the similar temperature range χ_1^R shows hump like behavior (as shown in Fig. 4). This behavior is evocative of χ_3^R as observed in spin glass (SG) [40,49,53] and superparamagnetic (SPM) systems [41,47,54]. However, unlike SG, in this case, χ_3^R does not show any critical behavior with respect to applied magnetic field, frequency and temperature. Moreover, the temperature-dependent behavior of χ_1 and χ_3 follow the Wohlfarth model [41,47,50,54]. The ac-field-dependent behavior of $|\chi_3^R|$ is shown in the right-hand side upper inset of Fig. 7(a) and the value of $|\chi_3^R|$ approaches towards saturation with decreasing the amplitude of ac-field, which is a clear indication of the blocking phenomena of magnetic clusters. According to the Wohlfarth SPM model [54], the magnetization (M) of a non-interacting single domain SPM particle is represented as

$$M = n\bar{\mu}L\left(\frac{\bar{\mu}}{k_B T}\right), \tag{1}$$

where n is the number of particles per unit volume, $\bar{\mu}$ is the average magnetic moment of a single magnetic entity or particle, k_B is the Boltzmann's constant, and $L(x)$ is the Langevin function. So, from Eq. (1), the linear susceptibility can be expressed as

$$\chi_1^R = \frac{\bar{\mu}}{3k_B T} \tag{2}$$

and the third-order susceptibility is represented as

$$\chi_3^R = -\left(\frac{n\bar{\mu}}{45}\right)\left(\frac{\bar{\mu}}{k_B T}\right)^3. \tag{3}$$

Therefore Eqs. (2) and (3) demonstrate that in the SPM region χ_1^R is positive and it follows T^{-1} behavior, whereas χ_3^R is

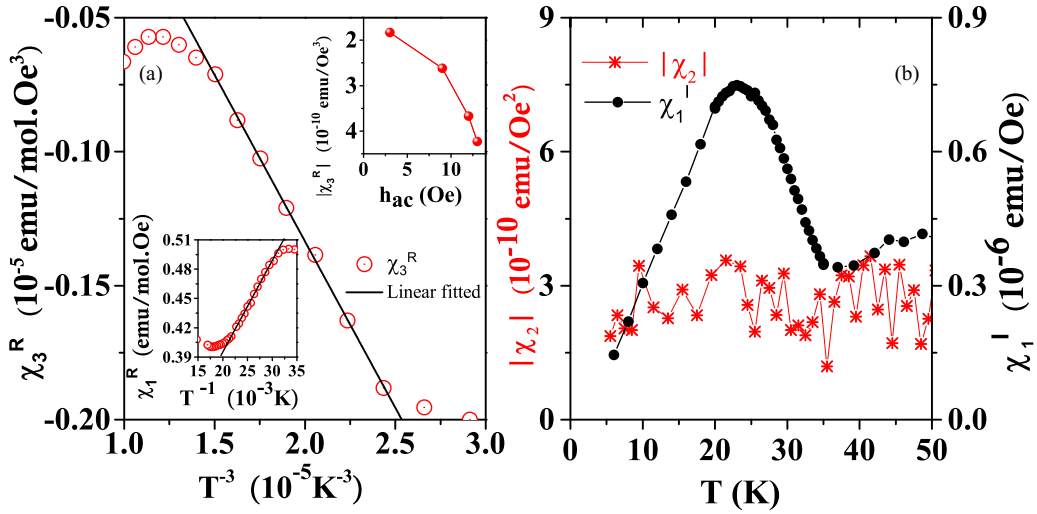

FIG. 7. (a) $|\chi_3^R|$ is plotted against T^{-3} and the black line shows the linear fitting. (Inset, top right) $|\chi_3^R|$ is plotted against amplitude of applied ac-magnetic field at temperature 33 K for the sample A3. (Inset, down left) χ_1^R is plotted against T^{-1} above the 32-K black line shows the linear fitting to the data. (b) Imaginary part of χ_1^I(right-hand side Y axis) and $|\chi_2|$ (left-hand side Y axis) are plotted against temperature of A3 composite. The measurements are performed at $h_{ac} = 12$ Oe at an exciting frequency of $f = 231.1$ Hz. Only in the top right inset of (a) the exciting ac field is varied at the same frequency.

negative and it follows T^{-3} behavior [54]. Figure 7(a) shows the T^{-3} temperature dependence for experimentally obtained χ_3^R and lower inset of Fig. 7(a) shows the T^{-1} dependency of χ_1^R above 32 K. The value of $\bar{\mu}$ ($\sim 10^3$ μ_b, μ_b is Bohr magneton) is calculated from the slope ratio obtained from the straight line fitting of χ_3^R and χ_1^R. In case of a conventional SPM cluster (smaller particles of ferromagnet), the values of $\bar{\mu}$ are quite large (as it contains a large number of ferromagnetically align spins inside its volume, for a pure ferromagnetic clusters, it is of the order of 10^4–$10^6 \mu_b$ [50]) compared to the number we have obtained from fitting. It indicates that the SPM clusters are not ferromagnetic in nature. Moreover, no anomaly in the temperature-dependent $|\chi_2|$ measurement is observed throughout the temperature interval as shown in Fig. 7(b) (scale: Left-hand Y axis scale), indicating a zero value of internal field (i.e., nonferromagnetic type clusters). Figure 7(b) also shows the temperature-dependent plot of χ_1^I (scale: right-hand Y axis scale), below 33 K, a humplike feature is observed in χ_1^I graph and no further anomaly in χ_1^I is observed above 33 K. χ_1^I corresponds to the imaginary part of the first-order ac susceptibility and signifies an area of a minor magnetic hysteresis loop [35], which does not show any anomaly both around and above blocking temperature T_B. Therefore all these observations are ruling out the possibility of forming a ferromagnetic type of clusters around $T_{S(\text{onset})}$. In ac-susceptibility measurements at the zero dc bias field, the AFM type ordered systems (or clusters) show a zero value of the internal field (i.e., $|\chi_2| = 0$) and a null value of a minor hysteresis loop area (i.e., $\chi_1^I = 0$) [51], which is similar to our observations. Therefore the fundamental and higher order susceptibility measurements confirm the excess susceptibility or a hump in χ_1^R around $T_{S(\text{onset})}$ appears due to the blocking of the SPM type AFM clusters.

SPM clusters are short-range-ordered magnetic clusters and its anisotropy energy is comparable to the thermal energy. Due to this reason the clusters show dynamical behavior above blocking temperature but the microscopic spin structure or the interaction between the spins remain the same to that of the long-range-ordered magnetic structure or state [41]. These short-range-ordered AFM clusters can appear from the covalent bonding between Cu^{+2} ions and Co^{+3} or Co^{+4} ions across the interface, as it is observed in YBCO/LCMO heterostructure [14,15]. However, in our case, the large suppression of the diamagnetic fraction [shown in Fig. 4(b)] along with the significant change of χ_1^R(T) around $T_{S(\text{onset})}$ ($\sim 10^{-5}$ emu, shown in Fig. 4) indicates the perturbation is not only confine to the interface but it is propagated well inside the bulk of LCu, i.e., the bulk magnetic property of LCu is modulated due to close proximity of LCo. Recently, the emergence of bulk CDW phase is evident in cuprate/ferromagnet heterostructure [16,17] and the appearance of similar CDW phase, AFM phase, and AFM glass phase is also evident while the superconductivity of a cuprate is destroyed by applying very high magnetic field or by applying very high strain on it [8–10,55–58]. Here we have observed formation of the short-range-ordered SPM type AFM clusters along with decrement of diamagnetic fraction which are unrelated to change in crystal structure or change of charge carrier concentration. Hence, the most probable reason is, the AFM fluctuation of LCu is suppressed by the exchange magnetic field of LCo. The exchange bias field can propagate through the covalent bonding between Cu^{+2} ions and Co^{+3} or Co^{+4} ions across the interface or directly inside LCu, and resulted in the formation of short-range-ordered SPM type AFM clusters both across the interface and also within the bulk of LCu.

The presence of AFM type spin fluctuation in optimally doped LCu has already been found from various measurements like specific heat, neutron diffraction, x-ray scattering [1–3,7–10,31–33], etc. In this section, we are going to emphasize on the phenomena related to exchange magnetic field stabilized AFM ordering in cuprate superconductor. For that, a small dc bias field is superimposed with the ac field during the

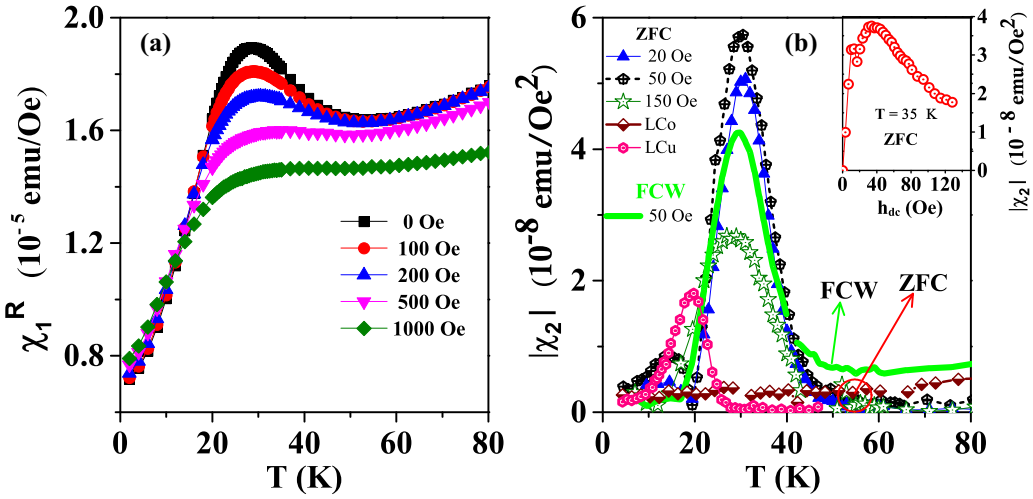

FIG. 8. (a) χ_1^R data of A3 are plotted against the temperature in five superimposed dc fields 0, 100, 200, 500, and 1000 Oe. (b) $|\chi_2|$ graph of A3 is shown in three superimposed dc fields 20, 50, and 150 Oe. The measurements are performed in ZFC and FCW (green bold line), the plots for LCu and LCo are also shown at 50 Oe superimposed dc field in the ZFC mode. (Inset) The isotherm of $|\chi_2|(H)$ of A3 at $T = 35$ K. For all measurement, the amplitude and frequency of the ac field are $h_{ac} = 12$ Oe and $f = 231.1$ Hz.

susceptibility measurements. Figure 8(a) shows the dc field superimposed $\chi_1^R(T)$ plot of composite A3, the peak value of χ_1^R(T) suppress and the peak temperature (corresponding to the blocking temperature T_B) shifts towards higher temperature [$\Delta(T_B) \sim 6$ K] with increasing the amplitude of dc bias field. The applied maximum dc bias filed (h_{max}) is very small in magnitude, hence the Zeeman energy does not have sufficient strength to disturb the already formed AFM clusters in LCu, but the magnetic response of LCo can be manipulated. At a very lower value of the dc bias field, the loosely coupled surface spins are responding and when the dc-field amplitude exceeds the value of demagnetization field of the ferromagnet (∼50 Oe), then spins at the bulk of LCo are responding, because above the demagnetization field Zeeman energy overcome the magnetocrystalline anisotropy energy and hence the cobalt spins align along a resultant direction decided by the competition between these two interactions. As the cobalt spins are coupled with the copper spins by exchange force, therefore the effective exchange bias field on LCu created by LCo also changes due to the change of orientation of cobalt spins. Thus the preformed AFM clusters feel this change and get biased indirectly by this small value of applied dc field, and hence the decrement of relaxation peak height of $\chi_1^R(T)$ and the positive increment of T_B with increasing the amplitude of dc bias field is observed.

To further emphasize on this exchange bias model the dc-field superimposed second-order susceptibility (χ_2) measurements are performed, as the application of dc bias field tunes the amplitude of effective exchange bias field seen by the copper spins of LCu. The copper spins are at different distances from the interface hence, each spins of LCu is going to feel different amplitude of exchange force created by the cobalt spins. So, the internal spin arrangement of the antiferromagnetic clusters in LCu is not going to remain the same as the previous case of $h_{dc} = 0$ Oe. Therefore these change of the internal field amplitude is going to reflect on the second order susceptibility ($|\chi_2|$). The dc-field superimposed temperature-dependent $|\chi_2|$ measurement [$|\chi_2|$(T)] is shown in Fig. 8(b). The anomaly in $|\chi_2|$(T) appears around 50 K and persists up to 5 K. These measurements are performed in ZFC (zero field cooled) mode, the sample is cooled in zero field and all measurements are performed in warming cycle in the presence of dc field $h_{dc} = 20$, 50, and 150 Oe, respectively). One of the graph in Fig. 8(b) (green bold line) corresponds to the FCW (field cool warming) measurements taken at $h_{dc} =$ 50 Oe. In this protocol, the dc field is applied above T_C of A3, then cooled to 5 K and measurements are performed during warming cycle in the presence of same dc field (50 Oe). In ZFC measurements, initially the peak value of $|\chi_2|(T)$ [Fig. 8(b)] increases up to dc-field of amplitude 50 Oe and then it decreases with further increasing the amplitude of the dc bias field. The inset shows the isotherm of $|\chi_2|$ [i.e., $|\chi_2|(H)$] at 35 K, revealing the same details as obtained from $|\chi_2|(T)$, viz. $|\chi_2|$ decreases after a particular field (50 Oe). Similar measurements are performed for the parent ingredients, but no anomaly in $|\chi_2|$ is observed around these temperatures (i.e., 20–50 K). The $|\chi_2|$(T) graph of LCu depicts the appearance of $|\chi_2|$ below about 25 K. (In case of the cuprate superconductor, a magnetic field-dependent critical current density is the source of $|\chi_2|$ [36–38]) and in the case of LCo, $|\chi_2|$ appears around $T_C \sim 233$ K, because of the appearance of the internal symmetry breaking field but much below T_C $|\chi_2|$ shows almost a zero value because of the domination of the demagnetization effect, so neither LCo nor LCu alone is responsible for the anomaly observed in $|\chi_2|$ around 35 K for the composites.

This anomalous variation of $|\chi_2|$ with the dc field can be very nicely explained by using the exchange coupling model. The mathematical form to describe exchange coupling between two magnetic material across the interface is as follows [59–62]:

$$H_{ex} = -j\frac{S_{AFM} \times S_{FM}}{\mu \times t_{FM} \times M_{FM}}. \quad (4)$$

Here, H_{ex} is the exchange bias field, J is the exchange integral across the FM/AFM interface per unit area, S_{AFM} and S_{FM} are the interface (or surface) magnetization amplitude of the

antiferromagnet and the ferromagnet, respectively, t_{FM} is the thickness of the ferromagnetic domain, and M_{FM} is the magnetization of the FM layer at a magnetic filed "*h*." At lower value of dc bias field (<50 Oe), the spins across the interface are only going to respond (i.e., S_{FM}, as they are loosely coupled to the bulk of LCo), whereas the bulk magnetization are not going to respond at this lower value of dc field, i.e., M_{FM} and t_{FM} remain unchanged (because the applied field amplitude is still lower than the values of demagnetization field). Therefore, according to Eq. (4) at lower dc-field amplitude, the effective H_{ex} (local field) on copper spins is larger in amplitude, which causes comparatively sizable misalignment between the AFM coupled copper spin, as they are at different distance from the interface. Due to this reason the increment of $|\chi_2|$ is observed up to a certain value of dc magnetic field (i.e., 50 Oe). On further increasing the dc-field amplitude, the bulk spins start to respond, because it exceeds the amplitude of demagnetization field of LCo (i.e., M_{FM} and t_{FM} increases simultaneously), as a result M_{FM} and t_{FM} start to dominant over S_{FM}, and hence, H_{ex} reduces in accordance with Eq. (4). As a result the misalignment between the copper spins reduces and decrement of $|\chi_2|$ is observed at higher value of dc bias field. Similarly, the difference of $|\chi_2|$(T) values between ZFC and FCW protocol [shown in Fig. 8(b)] can also be explained by using Eq. (4). As the ferromagnetic domain size (t_{FM}) and M_{FM} of LCo in the FCW condition is larger than the ZFC condition (below saturation field), evident from higher value of $|\chi_2|$ in the case of FCW than ZFC above 50 K, i.e., higher value of the internal field, hence the resultant exchange bias field values on copper spins is larger in the ZFC case than the FCW case. As a result the observed values of $|\chi_2|$(T) below 50 K is lower in the FCW case than it is in ZFC case. This observation further supports the proposed exchange bias model. Additionally, a measurement of the minor magnetic hysteresis loop, which is discussed in Sec. B [45] also shows evidence of an exchange bias between the copper and cobalt spins.

These preformed SPM type AFM clusters are also observed to affect the superconducting state of LCu. Hence, a comprehensive understanding of the evolution of superconductivity in these composites requires information on the critical thermodynamic parameters such as critical field (H_{C2}) and critical current density (J_C) of LCu. H_{C2} and J_C are affected because of disorder and while the system size becomes comparable to certain characteristic's length scale, like coherence length (ξ_0) and London penetration depth(λ_l) [63–65]. Here the imaginary part of χ_1 (χ_1^I) has been used as a probing tool to realize the nature of H_{C2} and J_C. In ac-susceptibility measurements, the phase lag between the ac-driving field and corresponding magnetization results in χ_1^I. In case of a type-2 superconductor χ_1^I appears around $T_{S(\text{onset})}$ because of vortex formation and pinning of it [66–68]. The maximum point of χ_1^I represents the temperature (T_S) at which the bulk superconductivity vanishes, i.e., the critical current density (J_C) $\longrightarrow$ 0 and the applied magnetic field fully penetrates inside the superconductor [35,66–68]. According to Bean model [35], the hysteresis loss (W) is inversely proportional to the critical current density (J_C), hence, at $T \longrightarrow T_S$, $J_C \longrightarrow 0$, so W diverges at T_S, as a result of that at $T = T_S$ peak in χ_1^I is observed [35–37]. The dc-field-dependent behavior of χ_1^I around $T_{S(\text{onset})}$ describes the anomaly is because of superconductivity [35] (see Sec. C in Ref. [45]). The temperature-dependent χ_1^I plot of A2, A3 and A4 are shown in Fig. 9(a). The onset point of χ_1^I for A3, A4, and A2 are observed around 34, 31, and 30 K respectively, whereas the diverging temperature of χ_1^I is observed at ∼24.5, ∼20, and ∼19 K for A3, A4, and A2, respectively. The crystalline size of LCu is same for all composites (as previously discussed), therefore according to the Bean model and H_C, T_S, and J_C phase diagram of a superconductor [35–37], the maximum point of χ_1^I is decided by the strength of the critical current density. In case of A3, the maximum point of χ_1^I is observed at higher temperature than A2 and A4, which clearly indicates that the strength of critical current density is highest in the case of composite A3, and according to the obtained temperature values, the amplitude of critical current density of the three composites can be expressed in the following descending order, i.e., $J_C(A3) > J_C(A4) > J_C(A2)$. Therefore, at any particular temperature below $T_{S(\text{onset})}$, the amplitude of critical field required to destroy the superconductivity is also highest for the corresponding material having highest value of critical current density. The plot of H_{C2} against T_S for A3, A2, and A4 is shown in Fig. 9(b), where H_{C2} can also be written in the following descending order $H_{C2}(A3) > H_{C2}(A4) > H_{C2}(A2)$. Therefore all these results are indicating that the composites having larger AFM volume fraction show smaller diamagnetic fraction (discussed previously in Fig. 4) and largest values of H_{C2} and J_C. This kind of unusual increase of the amplitude of critical thermodynamical parameters and decrease of diamagnetic fraction (shown in Fig. 4(b)) is often observed in the quantum size regime of superconductors, known as quantum size effect (QSE). The QSE model was proposed by DeGennes and Tinkham [63–65], where the mathematical expression for critical field (H_{C2}), critical current density (J_C), and effective London penetration depth (λ_{eff}) in the quantum limit can be represented as [63,64]

$$H_{C2} \sim \frac{\xi_0 \lambda_l}{r^{1.5}}, \tag{5}$$

$$J_C \sim \frac{1}{r^3}, \tag{6}$$

$$\lambda_{\text{eff}} = \lambda_l \left(1 + \frac{\xi_0}{r}\right)^{0.5}, \tag{7}$$

Here, $\xi_0 = \frac{0.18\hbar v_f}{k_B T_C}$ is the intrinsic coherence length, v_F Fermi velocity, λ_l London penetration depth, and $\mathbf{r}$ is the average size of the finite size superconducting clusters. According to Eqs. (5) and (6) in the finite size regime the values of critical parameters are decided by the size of superconducting volume fraction, hence larger amplitude of H_{C2} (and J_C) in the case of A3 compared to A2 and A4 indicates the superconducting volume fraction is smaller in A3 compared to A2 and A4. According to Eq. (7) the effective London penetration depth also increases in the finite size region, which causes the reduction of the effective diamagnetic fraction (or Meissner fraction) and hence smaller value of the superconducting volume fraction have been observed in the case of A3 compared to A4 and A5 [as shown in Fig. 4(b)]. XRD results are already depicting that there is no change of the crystalline volume of LCu in any of the composite compared to parent LCu.

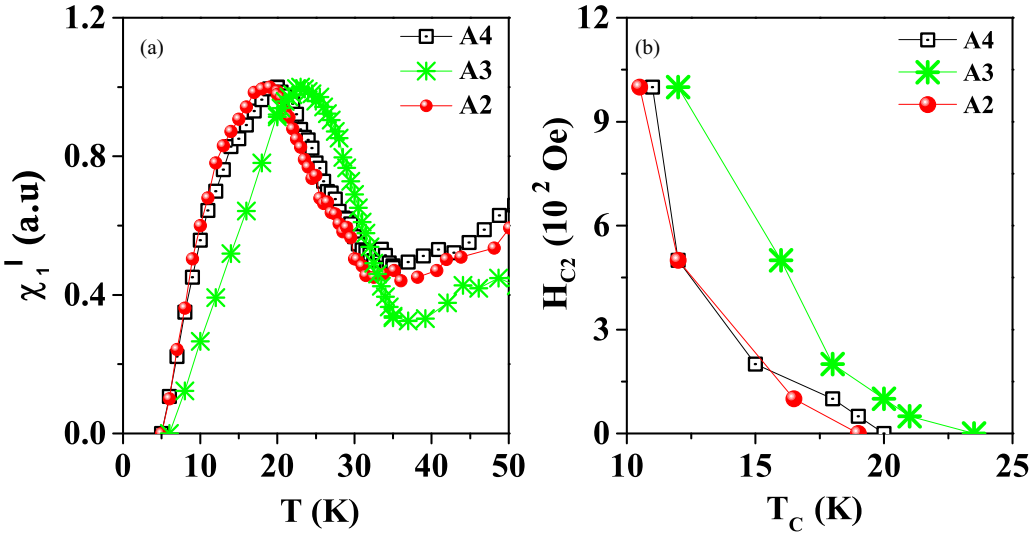

FIG. 9. (a) χ_1^I is plotted against temperature for A2, A3, and A4. (b) H_{C2} is plotted against temperature for A2, A3, and A4 composites.

So, the decrease of the superconducting volume fraction and the increase of H_{C2} and J_C are not due to the reduction of the crystalline size. Therefore the SPM type AFM clusters, which are formed within the bulk of LCu, reduce the superconducting volume fraction, as the microscopic spin structure of the corresponding SPM cluster is static in nature and can not support superconductivity. It is already known from previous studies that any kind of static magnetic structure is unfavorable for superconductivity in cuprate superconductors, because the superconducting state of a cuprate evolves after diluting the antiferromagnetic network and only the dynamic AFM fluctuation can sustain with superconducting ordering [1–3]. Therefore these observations are suggesting that the whole superconducting volume is divided into two phase separated regions, one phase consists of isolated SPM type AFM clusters and another phase is the finite size superconducting clusters.

So, from all the above discussion, it can be claimed that when AFM fluctuation is stabilized by the exchange magnetic field of LCo, the AFM order emerges, and superconducting volume fraction suppresses. This clearly indicates that the AFM type fluctuation can be a mediator of superconductivity in cuprate superconductor indicating that it is taking part in Cooper pairing.

V. CONCLUSION

A composite of a superconductor (LCu) and a ferromagnet (LCo) has been prepared by the solid state reaction method. In ac-susceptibility measurements, an anomaly is observed above $T_{S(\text{onset})}$ and it has been proved as the interface effect by changing the effective interface between LCu and LCo. It is proved through the studies of the linear (χ_1) and nonlinear ac susceptibilities (χ_2, χ_3) that the exchange field of LCo affects the copper spins and stabilizes the short-range-ordered AFM state within the bulk of LCu. These observations unambiguously indicates that the dynamic AFM fluctuation can be the mediator of copper pairing in cuprate superconductor substantiated by the observation of reduction of superconducting volume fraction when the AFM fluctuations are stabilized by the formation of the stable short-range-ordered SPM type AFM phase within the bulk. Further, the superconducting volume fraction reduce to the quantum size limit and two phase separated regions are formed, one is superparamagnetic type AFM clusters and the rest is finite size superconducting volume. Another important inference is that the reduced superconducting volume fraction shows quantum size effect (according to the DeGennes and Tinkham model), which is otherwise very difficult to achieve by preparing the nanoparticle of LCu, because of the structural limitation and degradation of oxygen stoichiometry. So these composites provide a unique path to understanding the mechanism of Cooper pairing and also opens up a pathway to study the physical property of the finite size superconducting clusters of cuprate superconductors.

ACKNOWLEDGMENTS

We acknowledge Dr. Mukul Gupta and Dr. N. P. Lalla for XRD measurements. Kranti Kumar Sharma and Dr. Santanu De are acknowledged for discussion and help during measurements. We are thankful to IRCC IIT Bombay MEMS department for TEM measurement.

[1] C. M. Varma, Rev. Mod. Phys. **92**, 031001 (2020).
[2] D. J. Scalapino, Rev. Mod. Phys. **84**, 1383 (2012).
[3] M. P. M. Dean, G. Dellea, R. S. Springell, F. Yakhou-Harris, K. Kummer, N. B. Brookes, X. Liu, Y.-J. Sun, J. Strle, T. Schmitt *et al.*, Nat. Mater. **12**, 1019 (2013).
[4] K. Yamada, C. H. Lee, K. Kurahashi, J. Wada, S. Wakimoto, S. Ueki, H. Kimura, Y. Endoh, S. Hosoya, G. Shirane, R. J. Birgeneau, M. Greven, M. A. Kastner, and Y. J. Kim, Phys. Rev. B **57**, 6165 (1998).
[5] A. V. Balatsky and P. Bourges, Phys. Rev. Lett. **82**, 5337 (1999).

[6] S. Wakimoto, K. Yamada, J. M. Tranquada, C. D. Frost, R. J. Birgeneau, and H. Zhang, Phys. Rev. Lett. **98**, 247003 (2007).

[7] G. Aeppli, T. E. Mason, S. M. Hayden, H. A. Mook, and J. Kulda, Science **278**, 1432 (1997).

[8] J. M. Tranquada, B. J. Sternlieb, J. D. Axe, Y. Nakamura, and S. Uchida, Nature (London) **375**, 561 (1995).

[9] J. M. Tranquada, J. D. Axe, N. Ichikawa, Y. Nakamura, S. Uchida, and B. Nachumi, Phys. Rev. B **54**, 7489 (1996).

[10] J. M. Tranquada, J. D. Axe, N. Ichikawa, A. R. Moodenbaugh, Y. Nakamura, and S. Uchida, Phys. Rev. Lett. **78**, 338 (1997).

[11] V. A. Vas'ko, V. A. Larkin, P. A. Kraus, K. R. Nikolaev, D. E. Grupp, C. A. Nordman, and A. M. Goldman, Phys. Rev. Lett. **78**, 1134 (1997).

[12] V. Peña, Z. Sefrioui, D. Arias, C. Leon, J. Santamaria, J. L. Martinez, S. G. E. te Velthuis, and A. Hoffmann, Phys. Rev. Lett. **94**, 057002 (2005).

[13] V. Peña, Z. Sefrioui, D. Arias, C. Leon, J. Santamaria, M. Varela, S. J. Pennycook, and J. L. Martinez, Phys. Rev. B **69**, 224502 (2004).

[14] J. Chakhalian, J. W. Freeland, G. Srajer, J. Strempfer, G. Khaliullin, J. C. Cezar, T. Charlton, R. Dalgliesh, C. Bernhard, G. Cristiani, H.-U. Habermeier, and B. Keimer, Nat. Phys. **2**, 244 (2006).

[15] D. K. Satapathy, M. A. Uribe-Laverde, I. Marozau, V. K. Malik, S. Das, Th. Wagner, C. Marcelot, J. Stahn, S. Brück, A. Rühm, S. Macke, T. Tietze, E. Goering, A. Frañó, J.-H. Kim, M. Wu, E. Benckiser, B. Keimer, A. Devishvili, B. P. Toperverg, M. Merz, P. Nagel, S. Schuppler, and C. Bernhard, Phys. Rev. Lett. **108**, 197201 (2012).

[16] N. Driza, S. Blanco-Canosa, M. Bakr, S. Soltan, M. Khalid, L. Mustafa, K. Kawashima, G. Christiani, H.-U. Habermeier, G. Khaliullin, C. Ulrich, M. Le Tacon, and B. Keimer, Nat. Mater. **11**, 675 (2012).

[17] A. Frano, S. Blanco-Canosa, E. Schierle, Y. Lu, M. Wu, M. Bluschke, M. Minola, G. Christiani, H. U. Habermeier, G. Logvenov, Y. Wang, P. A. van Aken, E. Benckiser, E. Weschke, M. Le Tacon, and B. Keimer, Nat. Mater. **15**, 831 (2016).

[18] J. He, P. Shafer, T. R. Mion, Vu Thanh Tra, Q. He, J. Kong, Y.-D. Chuang, W. L. Yang, M. J. Graf, J.-Y. Lin, Y.-H. Chu, E. Arenholz, and R.-H. He, Nat. Commun. **7**, 10852 (2016).

[19] J. Chakhalian, J. W. Freeland, H.-U. Habermeier, G. Cristiani, G. Khaliullin, M. van Veenendaal, and B. Keimer, Science **318**, 1114 (2007).

[20] K. Li and D. Xue, J. Phys. Chem. A **110**, 11332 (2006).

[21] H. Y. Hwang, Y. Iwasa, M. Kawasaki, B. Keimer, N. Nagaosa, and Y. Tokura, Nat. Mater. **11**, 103 (2012).

[22] J. Jeong, N. Aetukuri, T. Graf, T. D. Schladt, M. G. Samant, and S. S. P. Parkin, Science **339**, 1402 (2013).

[23] S. Komori, A. Di Bernardo, A. I. Buzdin, M. G. Blamier, and J. W. A. Robinson, Phys. Rev. Lett. **121**, 077003 (2018); I. Bozovic, G. Logvenov, I. Belca, B. Narimbetov, and I. Sveklo, *ibid.* **89**, 107001 (2002); J. P. Locquet, J. Perret, J. Fompeyrine, E. Machler, J. W. Seo, and G. Van Tendeloo, Nature (London) **394**, 453 (1998).

[24] D. Hsu, T. G. Kumary, L. Lin, and J. G. Lin, Phys. Rev. B **74**, 214504 (2006).

[25] N. Biškup, S. Das, J. M. Gonzalez-Calbet, C. Bernhard, and M. Varela, Phys. Rev. B **91**, 205132 (2015).

[26] S. Das, K. Sen, I. Marozau, M. A. Uribe-Laverde, N. Biskup, M. Varela, Y. Khaydukov, O. Soltwedel, T. Keller, M. Döbeli, C. W. Schneider, and C. Bernhard, Phys. Rev. B **89**, 094511 (2014).

[27] M. Itoh, I. Natori, S. Kubota, and K. Motoya, J. Magn. Magn. Mater. **140**, 1811 (1995).

[28] J. Wu and C. Leighton, Phys. Rev. B **67**, 174408 (2003).

[29] P. S. Anil Kumar, P. A. Joy, and S. K. Date, J. Phys.: Condens. Matter **10**, L487 (1998).

[30] V. K. Malik, C. H. Vo, E. Arenholz, A. Scholl, A. T. Young, and Y. Takamura, J. Appl. Phys. **113**, 153907 (2013).

[31] C. Panagopoulos, B. D. Rainford, J. R. Cooper, and C. A. Scott, Physica C **341**, 843 (2000).

[32] M.-H. Julien, A. Campana, A. Rigamonti, P. Carretta, F. Borsa, P. Kuhns, A. P. Reyes, W. G. Moulton, M. Horvatić, C. Berthier, A. Vietkin, and A. Revcolevschi, Phys. Rev. B **63**, 144508 (2001).

[33] C. Panagopoulos, J. L. Tallon, B. D. Rainford, T. Xiang, J. R. Cooper, and C. A. Scott, Phys. Rev. B **66**, 064501 (2002).

[34] B. Dutta, K. Kumar, and A. Banerjee, AIP Conf. Proc. **2115**, 030515 (2019).

[35] C. P. Bean, Rev. Mod. Phys. **36**, 31 (1964).

[36] P. W. Anderson and Y. B. Kim, Rev. Mod. Phys. **36**, 39 (1964).

[37] G. R. Kumar and P. Chaddah, Phys. Rev. B **39**, 4704 (1989).

[38] K. H. Müller, J. C. Macfarlane, and R. Driver, Physica C **158**, 366 (1989).

[39] D. Bhattacharya, L. C. Pathak, S. K. Mishra, D. Sen, and K. L. Chopra, Appl. Phys. Lett. **57**, 2145 (1990).

[40] A. Bajpai and A. Banerjee, Phys. Rev. B **55**, 12439 (1997).

[41] A. Bajpai and A. Banerjee, Phys. Rev. B **62**, 8996 (2000).

[42] S. Mukherjee and R. Ranganathan, Phys. Rev. B **54**, 9267 (1996).

[43] T. Satō and Y. Miyako, J. Phys. Soc. Jpn. **51**, 1394 (1982).

[44] S. Fujiki and S. Katsura, Prog. Theor. Phys. **65**, 1130 (1981).

[45] See Supplemental Material at http://link.aps.org/supplemental/10.1103/PhysRevB.106.134520 for the (A) elaborate analysis of transmission electron data, (B) minor magnetic loop graph, and (C) dc-field-dependent imaginary part of first-order ac-susceptibility (χ_1^I) measurements.

[46] B. Dutta, K. Kumar, N. Ghodke, and A. Banerjee, Rev. Sci. Instrum. **91**, 123905 (2020); A. Bajpai and A. Banerjee, *ibid.* **68**, 4075 (1997).

[47] T. Bitoh, K. Ohba, M. Takamatsu, T. Shirane, and S. Chikazawa, J. Magn. Magn. Mater. **154**, 59 (1996); S. Mukherjee, R. Ranganathan, and S. B. Roy, Solid State Commun. **98**, 321 (1996); A. Chakravarti, R. Ranganathan, and C. Bansal, *ibid.* **82**, 591 (1992).

[48] G. Sinha and A. Majumdar, J. Magn. Magn. Mater. **185**, 18 (1998).

[49] K. Binder and A. P. Young, Rev. Mod. Phys. **58**, 801 (1986).

[50] A. Bajpai and A. Banerjee, J. Phys.: Condens. Matter **13**, 637 (2001); A. K. Pramanik and A. Banerjee, Phys. Rev. B **82**, 094402 (2010).

[51] S. Nair and A. Banerjee, Phys. Rev. Lett. **93**, 117204 (2004).

[52] S. Nair and A. Banerjee, Phys. Rev. B **68**, 094408 (2003).

[53] M. Suzuki, Prog. Theor. Phys. **58**, 1151 (1977).

[54] E. P. Wohlfarth, Phys. Lett. A **70**, 489 (1979).

[55] A. J. Achkar, R. Sutarto, X. Mao, F. He, A. Frano, S. Blanco-Canosa, M. Le Tacon, G. Ghiringhelli, L. Braicovich, M. Minola, M. Moretti Sala, C. Mazzoli, Ruixing Liang, D. A. Bonn, W. N. Hardy, B. Keimer, G. A. Sawatzky, and D. G. Hawthorn, Phys. Rev. Lett. **109**, 167001 (2012).

[56] A. J. Achkar, X. Mao, C. McMahon, R. Sutarto, F. He, R. Liang, D. A. Bonn, W. N. Hardy, and D. G. Hawthorn, Phys. Rev. Lett. **113**, 107002 (2014).
[57] S. Sachdev and E. Demler, Phys. Rev. B **69**, 144504 (2004).
[58] L. E. Hayward, D. G. Hawthorn, R. G. Melko, and S. Sachdev, Science **343**, 1336 (2014).
[59] W. H. Meiklejohn and C. P. Bean, Phys. Rev. **102**, 1413 (1956).
[60] D. Mauri, H. C. Siegmann, P. S. Bagus, and E. Kay, J. Appl. Phys. **62**, 3047 (1987).
[61] N. C. Koon, Phys. Rev. Lett. **78**, 4865 (1997).
[62] S. Karmakar, S. Taran, E. Bose, B. K. Chaudhuri, C. P. Sun, C. L. Huang, and H. D. Yang, Phys. Rev. B **77**, 144409 (2008).
[63] S. Bose and P. Ayyub, Rep. Prog. Phys. **77**, 116503 (2014).
[64] P. G. de Gennes and M. Tinkham, Phys. Phys. Fiz. **1**, 107 (1964).
[65] M. Tinkham, Phys. Rev. **110**, 26 (1958).
[66] L. Civale, T. K. Worthington, L. Krusin-Elbaum, and F. Holtzberg, in *Magnetic Susceptibility of Superconductors and Other Spin Systems*, edited by R. A. Hein, T. L. Francavilla, and D. H. Liebenberg (Plenum, New York, 1991), pp. 313–332, and references therein.
[67] X. Ling and J. I. Budnick, in *Magnetic Susceptibility of Superconductors and Other Spin Systems*, edited by R. A. Hein, T. L. Francavilla, and D. H. Liebenberg (Plenum, New York, 1991), pp. 377–388, and references therein.
[68] S. Ramakrishnan, R. Kumar, C. V. Tomy, A. K. Grover, S. K. Malik, and P. Chaddah, in *Magnetic Susceptibility of Superconductors and Other Spin Systems*, edited by R. A. Hein, T. L. Francavilla, and D. H. Liebenberg (Plenum, New York, 1991), pp. 389–404, and references therein.